Abbreviations

%N	percentage nitrogen by mass
2-NDPA	2-Nitrodiphenylamine
AO	atomic orbital
a.u.	atomic units
B3LYP	Becke, 3-parameter, Lee-Yang-Parr hybrid functional
BCP	bonding critical point
CH_3CH_3	NC repeat unit with two $-OCH_3$ capping groups
CH_3OH	NC repeat unit with $-OCH_3$ capping group on ring 1 and $-OH$ group on ring 2
CCP	cage critical point
CP	critical point
DFT	density functional theory
DSC	differential scanning calorimetry
DOS	degree of substitution
DPA	diphenylamine
ELF	electron localisation function
EM	energetic materials
EN	ethyl nitrate

ESP	electrostatic potential
G09	Gaussian 09 revision D.01
GM	genetically modified
GView	Gauss View 5.0.8
HF	Hartree-Fock
HMF	hydroxymethylfurfural
HOMO	highest occupied molecular orbital
IR	infra-red spectroscopy
LOL	localized orbital locator
MD	molecular dynamics
MEP	minimum energy path
MM	molecular mechanics
MMFF94	Merck molecular force field 94
MO	molecular orbital
MP2	Møller–Plesset perturbation theory with second order correction
MW	molecular weight
NC	nitrocellulose
NCP	nuclear critical point
NG	nitroglycerine
NMR	nuclear magnetic resonance spectroscopy
$OHCH_3$	NC repeat unit with $-OH$ capping group on ring 1 and $-OCH_3$ group on ring 2
PCM	polarisable continuum model

PES	potential energy surface
PETN	pentaerythritol tetranitrate
PETRIN	pentaerythritol trinitrate
QM	quantum mechanics
QTAIM	quantum theory of atoms in molecules
RCP	ring critical point
SB59	1,4-bis(ethylamino)-9,10-anthraquinone dye
SCF	self-consistent field
SEM	scanning electron microscopy
S_N2	bi-molecular nucleophilic substitution reaction
TG	thermogravitmetric analysis
TS	transition state
UFF	universal force field
UV	ultraviolet
UVvis	ultraviolet–visible spectroscopy
ωB97X-D	ωB97X-D long-range corrected hybrid functional
ZPE	zero-point energy

Chapter 1

Mechanisms of denitration under ambient conditions

1.1 Introduction

1.1.1 Thermolytic reactions

The first stage of thermolytic decomposition for nitrate esters is generally agreed to be homolytic fission of the O-N bond linking the nitrate to the alkyl chain, leading to the loss of $^{\cdot}NO_2$ (equation 1.1) [1, 2, 3]. Though nitrate homolysis is an endothermic reaction, the weak O-N bond has a typical dissociation enthalpy of 42 kcal mol^{-1} and is easily cleaved when exposed to elevated temperatures, UV light or impact. Whilst the thermolytic degradation of energetic materials has been widely studied experimentally, the ambient, slow ageing mechanisms are less well documented. Low-temperature decomposition routes are influenced by many factors over a protracted lifetime, and in practical use, materials are usually subject to evolving environmental conditions. External changes in pressure, humidity, stress and temperature cycling introduce variation in the degradation patterns of energetic materials. The presence of moisture has been observed to lower the activation energy and accelerate decomposition [2]. Internal factors including impurities, residual solvent, and crystal growth within the bulk, also alter decomposition behaviour.

$$\mathrm{R{-}ONO_2 \longrightarrow R{-}O^{\cdot} + {}^{\cdot}NO_2} \tag{1.1}$$

$$\mathrm{RH{-}ONO_2 \longrightarrow R{=}O + HNO_2} \tag{1.2}$$

The degradation of nitrate esters at temperatures over 100°C is primarily *via* thermolytic processes, whilst under 100°C, decomposition is largely thought to be the result of hydrolysis [5]. Tsyshevsky *et al.* studied the intramolecular reactions leading to denitration

1. $^{\bullet}NO_2$ loss
2. HNO_2 loss
3. OONO rearrangement
4. γ-attack
5. $ONO_2^{\bullet}$ loss
6. C−C cleavage ($CH_2O + NO_2$)
7. C−C cleavage ($CO + HNO_2$)

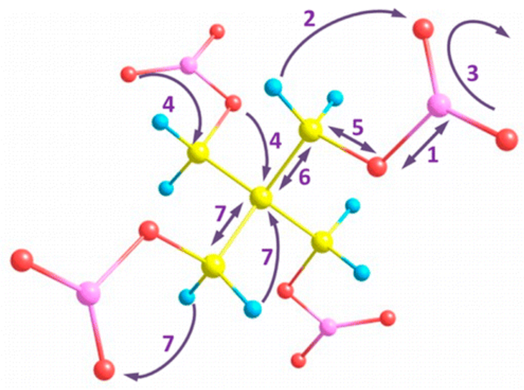

oxygen nitrogen carbon hydrogen

Figure 1.1: Intramolecular thermolytic reactions in pentaerythritol tetranitrate (PETN), from the work of Tsyshevsky *et al.* [4].

in pentaerythritol tetranitrate (PETN) in both the vacuum and the bulk crystal [4] (figure 1.1). Seven mechanisms for the removal of NO_2 were explored. Corresponding to the labels in figure 1.1: (1) homolytic cleavage of the $O{-}NO_2$ bond, (2) the elimination of nitrous acid (HNO_2) which is usually considered a competing reaction to homolytic fission, (3) the nitro-peroxynitrite rearrangement (O−ONO), (4) γ-attack of the terminating nitrate oxygen atom and the bridging nitrate oxygen at their relative γ-carbon sites, (5) the homolytic C−O bond cleavage, (6) and (7) two variations of the homolytic C−C bond cleavage.

It was found that the two most significant decomposition reactions were homolysis of the nitrate ester $O{-}NO_2$ bond (equation 1.1) and intramolecular elimination of HNO_2 (equation 1.2). Whilst elimination of HNO_2 was found to be the most energetically favourable denitration pathway, homolytic fission dominated preliminary decomposition steps due to the lower activation barrier and faster rate of reaction. It was suggested that global decomposition processes were determined by the interplay between these two mechanisms. Initial homolysis facilitated wide-spread denitration, complemented by exothermic HNO_2 elimination, promoting self-heating of the system and further bond dissociations. The presence of $^{\bullet}NO_2$ and HNO_2 have previously been linked to the autocatalytic rates observed for later-stage decomposition of nitrate esters [6, 7, 8], though some studies solely attribute it to the presence of acids [9, 10, 11, 12]. Other studies also implicate the action of $^{\bullet}NO$ and HNO_3, in addition to $^{\bullet}NO_2$ and HNO_2 [13, 14]. Inspection of these products generated from initial processes, with observation of the species permeating through to later stages, will shed light on the most likely contributors to autocatalysis.

1.1.2 Acid hydrolysis reactions

Spent acids remain in the nitrocellulose (NC) matrix following synthesis even with thorough washing procedures. Additional acidic species are released via the subsequent reactions of $^{\cdot}NO_2$ following homolysis. These acids proceed to react with other moieties in the system, such as unsubstituted alcohol side chains on the polysaccharide, or small molecules free in the bulk.

When exploring the interaction of nitroglycol and nitroglycerin in acid solution, Camera proposed a protonation-denitration scheme (scheme 1.1) whereby initial protonation at the nitrate is rapid (equation 1.3), but the subsequent release of the nitronium ion was slow and rate determining (equation 1.4).

$$CH_3CH_2ONO_2 + H^+ \xrightleftharpoons{\text{fast}} CH_3CH_2ONO_2H^+ \tag{1.3}$$

$$CH_3CH_2ONO_2H^+ \xrightleftharpoons{\text{slow}} CH_3CH_2OH + NO_2{}^+ \tag{1.4}$$

Scheme 1.1: The relative rate of stepwise protonation and denitration of nitrate esters, using ethyl nitrate as an example. From the work of Camera *et al.* [15].

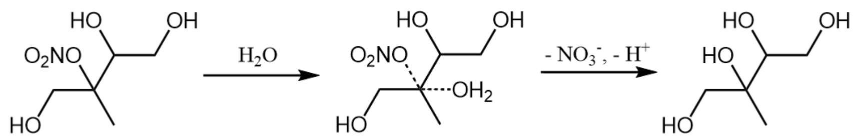

Scheme 1.2: Hydrolysis of a tertiary nitrate derived from the reaction of isoprene in the aerosol phase, from the work of Hu *et al.* [16].

NC in storage is kept wetted with solvents to prevent self-ignition. Material with 12.6%N or lower must be stored in 25% water by mass, or in a controlled mixture of solvents, stabilisers and plasticisers. The material is therefore always exposed to water, with the fast-exchange of protons expected at inter-facial surfaces. In the study of organonitrates and organosulfates generated from isoprene in the aerosol phase, Hu *et al.* found that primary and secondary nitrates were resilient to hydrolysis for pH > 0, whilst tertiary nitrates underwent hydrolytic nucleophilic substitution easily, reacting with water to form alcohols [16].

In tertiary nitrates, the carbon is fully substituted with no attached hydrogens. This group is usually sterically hindered and stabilising to carbocations, condition on the electron donation ability of the substituents remaining after nitrate removal. If formation of a carbocation intermediate is involved in the hydrolysis mechanism, this may explain why the tertiary nitrates exhibited highly efficient denitration, even under neutral conditions.

Though no specific mechanistic detail is given, the action of a protonated transition state during hydrolysis is alluded to through the contrast between the rate of acid-catalysed and neutral hydrolysis reactions. Neutral hydrolysis of the tertiary nitrates occured rapidly, but hydrolysis only occurred for primary and secondary nitrates under strongly acid catalysing conditions, and at a much slower rate. Additionally, the presence of adjacent OH groups hampered the rate of hydrolysis for some aerosol dispersed organonitrates. In the neutral hydrolysis of tertiary nitrates, increasing the number of adjacent OH groups lead to protracted hydrolysis lifetimes. Interestingly, the retardation effect of adjacent OH groups was not observed for the the acid catalysed cases. Hu proposed that this could be due to the interaction of OH with the transition state of the neutral hydrolysis system, compared to the protonated transition state of the acid catalysed system, impeding the reaction only in the former case. The cause of this effect is unclear, and without understanding of the mechanisms involved, it is difficult to explain.

There is evidence that nitration and denitration of nitrate esters is also influenced by the presence of nitrate groups at neighbouring positions. Matveev *et al.* demonstrated that for poly-nitroesters the rate of liquid-phase decomposition did not increase linearly with number of nitrate reaction centres. It was found to mainly dependend on individual structures (table 1.3) [17]. The trend in reactivity could be partially explained by the inductive effect of the nitro groups [1]. The inductive effect arises when a difference in the electronegativity between atoms connected by a σ bond leads to a polarisation, or permanent dipole, in the bond. Electron donating groups increase the δ^- partial charge on neighbouring atoms through the release of electrons, whilst electron withdrawing groups pull electron density away, generating a δ^+ charge on connected atoms. The NO_3 presents a stronger electron withdrawing effect than OH, which is a donating group. The presence of an adjacent nitrate appears to facilitate denitration, whereas the presence of hydroxyl groups hinders this process, for neutral hydrolytic schemes. The resonance effect, arising from π donation by lone pairs on oxygen and nitrogen is negligible between substituents at different sites on the polysaccharide ring, as the ring is saturated.

Table 1.1: Comparison of rate constants of decomposition for various polynitrate esters at 140°C. ΔT is the decomposition temperature range, E is the experimental activation barrier for decomposition, log$A$ is the pre-exponential factor, T_c is the combustion temperature, k_{expt} is the rate constant for decomposition. Collated from literature sources by Matveev *et al.*[17].

Compound	ΔT / °C	E / kcal mol^{-1}	log$A$ [s^{-1}]	k_{expt} / 10^{-6} s^{-1}
$O_2NOCH_2CH_2CH_2ONO_2$	72–140	39.1	14.9	1.7
$O_2NOCH_2CH_2CH_2CH_2ONO_2$	100–140	39.0	14.7	1.1
$O_2NOCH(CH_3)CH(CH_3)ONO_2$	72–140	40.3	14.9	5.0
$O_2NOCH_2CH_2OCH_2CH_2ONO_2$	80–140	42.0	16.5	1.9
$O_2NOCH_2CH(OH)(CH_2ONO_2)$	80–140	42.4	16.8	2.3
$O_2NOCH_2CH(ONO_2)(CH_3)$	72–140	40.3	15.8	3.0
$[(O_2NOCH_2)CH(ONO_2)CH(ONO_2)]_2$ (hexanitromannite)	80–140	38.0	15.9	63.0

The investigation by Hu *et al.* exclusively focused on nitrates generated from an isoprene precursor, upon dispersion as an aerosol. The nitrate groups present in NC are either of primary (C6) or secondary (C2, C3) structure, indicating that ambient hydrolysis is unlikely according to this scheme. However, solvent effects are expected to differ for condensed-phase reactions and aerosol phases. A greater build-up of acid concentration can be achieved in a closed, condensed system, and the lifetime of an aerosol is relatively short-lived when considering the timescale of slow ageing processes in NC. Thus, the work of Hu *et al.* does not provide a direct comparison for the NC polymer but highlights the possible contribution from both neutral and acid-catalysed hydrolysis routes, and effect of increasing levels of substitution on the wider structure.

In this section, the possible mechanisms for nitrate removal from the NC backbone are explored. The homolytic fission and HNO_2 elimination thermolytic processes suggested by Tsyshevsky will be compared to the acid hydrolysis scheme. Though the relative rates of reaction are not compared, the extended timescales involved in ambient ageing imply that the dominating reactions correspond to those most thermodynamically favourable.

1.2 Methodology

The energies of homolytic fission and elimination of HNO_2 were calculated for PETN, as a test system before extension to the NC monomer. The reaction energies were calculated according to equations 1.1 and 1.2 to reproduce the work of Tsyshevsky *et al.*; the published geometries of PETN and its derivatives were obtained from the authors. Whilst only the denitrated radical product geometry was provided in the case of the homolysis reaction, the product of HNO_2 elimination was given as a complex of the HNO_2 leaving group and the newly formed aldehyde. A single point energy and frequency calculation were performed on each of the species to determine the reaction energies; no geometry optimisation was performed on the given structures except for in the case the $^{\cdot}NO_2$ molecule, where the geometry was not supplied. A separate $^{\cdot}NO_2$ molecule was independently geometry optimised.

The intramolecular reactions of the NC monomer were modelled according to scheme 1.3. Rigid and relaxed potential energy surface (PES) scans were attempted for both reactions for the NC monomer to obtain an energy profile, and in the case of HNO_2 elimination, identify a transition state. The homolysis reaction was treated as barrierless. Where the scans were unable to identify a valid transition state geometry, guess transition state geometries were constructed and optimised.

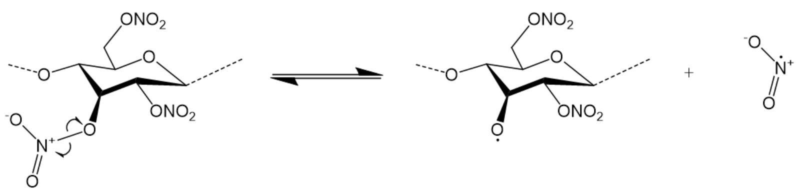

(a) Removal of a nitrate group *via* homolytic fission of NC

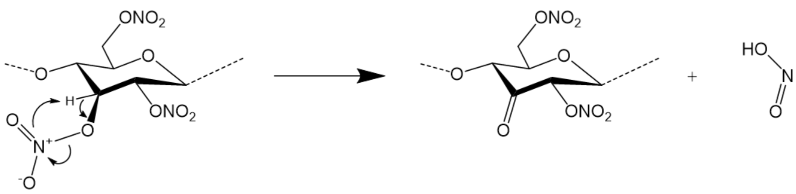

(b) Removal of a nitrate group *via* elimination of HNO_2.

Scheme 1.3: The proposed intramolecular reactions for the initial denitration step during NC degradation.

The possible protonation sites for the NC monomer were explored by placing a proton at each of the different oxygen sites surrounding the nitrate group. The structures were then geometry optimised and energies of protonation were compared. H_3O^+ was modelled as the donating species; as NC is usually stored wetted in water, the hydronium ion is the most likely source of protons. It is also possible that the proton is donated by other acidic species in the system, particularly HNO_2 or HNO_3. This is more likely at later stages of degradation when a higher concentration of acid has been generated by secondary reactions.

1.2.1 Computational details

All geometry optimisations, thermochemistry calculations and PES scans were performed in Gaussian 09 revision D.01 (G09). Geometry optimisation and thermal calculations were to the level of 6-31+G(2df,p). NC monomer structures were optimised using ωB97X-D long-range corrected hybrid functional (ωB97X-D), Becke, 3-parameter, Lee-Yang-Parr hybrid functional (B3LYP) and Møller–Plesset perturbation theory with second order correction (MP2). ΔG values were obtained by the difference between the thermally corrected free energies of products and reactants. Zero-point corrected energies ZPE were determined by addition of individual zero-point energy (ZPE) to the free energy:

$$\Delta G^{ZPE} = \sum(G_{products} + ZPE_{products}) - \sum(G_{reactants} + ZPE_{reactants}) \tag{1.5}$$

PES scans were performed to the level of ωB97X-D/6-31+g(d), or using unrestricted ωB97X-D, in the case of $O-{}^{\bullet}NO_2$ dissociation. Rigid scans were carried out by fixing bond lengths, angles and dihedral values as constants. Only the variable of interest was allowed to change. This was with the exception of relaxation of other specified coordinates required for accommodation of the new geometry, following each step of the scan. For example, in the homolysis of the nitrate $O-NO_2$ bond, as the NO_2 group departed, the internal O–N–O angle was also allowed to relax, in addition to the angle of the departing NO_2 with respect to the remainder of the molecule. In two-dimensional scans, two variables were scanned simultaneously. For the same reaction, the elongation of a the $O-NO_2$ bond was scanned with simultaneous approach of a proton, to monitor the effect of protonation for the same reaction. Relaxed scans were performed in Gaussian using the "modredundant" function, whereby the whole structure was geometry optimised after each step of the scan. Scans were performed with step size of 0.1 Å. The number of steps varied with the property investigated, though the majority of the phenomena were observed within 20 steps (2 Å). Scans were attempted in vacuum, and for the protonation cases, implicit solvent using polarisable continuum model (PCM) [18].

1.3 Results and discussion

1.3.1 Thermolytic decomposition mechanisms

The energies of homolytic fission and intramolecular elimination of HNO_2 from a PETN nitrate group are shown in table 1.2. The energy values published by Tsyshevsky *et al.* are denoted in parenthesis. The ΔG_r and E_a values are the same.

Despite using the author supplied geometries, same method and basis, it can be seen that the obtained PETN reaction energy in the case of homolytic fission ($^{\cdot}NO_2$ loss) varies greatly from the value published by Tsyshevsky *et al.* It was assumed that the supplied geometries were those used to generate the energy values quoted in their study. Inspection of the forces for the given structures showed that they were not converged. As the same structures were used to calculate values listed in table 1.2, the unconverged geometries do not explain the large discrepancy between the published energies and values obtained here. A contribution may arise from different compilations of the G09 program, leading to fluctuations in the exact values obtained. These differences would be amplified when combining individual energies during the calculation of reaction energy values, but are still not expected to account for the 20 kCal mol^{-1} deficiency in the case of homolysis.

A possible explanation is that the products of homolytic fission were treated as a complex, rather than individual molecules, though this was not highlighted in the original publication nor explicit in the supplied geometries. In the current study, the $^{\cdot}NO_2$ leaving group was independently geometry optimised, with its energy contributing additively to the products of the reaction. Under this assumption, the product species would move apart immediately following fission. If the energy of the product species were calculated separately

Table 1.2: Calculated free energies of reaction (ΔG_r), reaction enthalpies (ΔH_r), activation barriers (E_a) with zero-point correction (^{ZPE}) for the intramolecular reactions of PETN, and the NC monomer. Values expressed in kCal mol^{-1}.

Reaction	ΔG_r	ΔG_r^{ZPE}	ΔH_r	E_a	${E_a}^{ZPE}$
PETN					
$^{\cdot}NO_2$ loss	21.51	16.56	35.62	21.51[b]	16.56
	(41.2)[a]	(35.8)		(41.2)	(35.8)
HNO_2 loss	−23.63	−26.21	−20.39	41.29	36.28
	(−18.6)			(47.3)	(42.7)
NC monomer					
$^{\cdot}NO_2$ loss	23.25	18.69	36.26	23.25	18.69
HNO_2 loss	−36.05	−39.42	−22.86	40.70	37.33

[a] values from the work of Tsyshevsky *et al.* [4].
[b] values for the activation energy and total energy of reaction are the same for bond dissociation via homolytic fission.

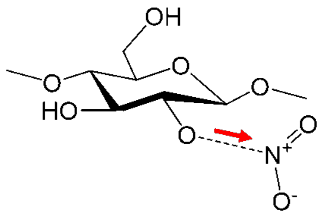

Figure 1.2: The $O-NO_2$ bond was elongated during rigid and relaxed PES scan to simulate homolytic fission for the NC monomer.

in the original study, it could be that the departing $^{\cdot}NO_2$ was not geometry optimised, but left in its complexed geometry. This is relevant in the scenario where the $^{\cdot}NO_2$ has not yet moved far enough from the remainder of the PETN molecule to fully relax. Whilst the calculated ΔG_r deviates greatly from the value in Tsyshevsky's study, the ΔH_r falls within 7kCal mol^{-1} of the literature value for $O-NO_2$ homolysis of alkanes (42±0.3 kCal mol^{-1}) [**?**].

The homolytic fission reaction was applied to a NC monomer singly nitrated at C2 (figure 1.2). The $O-NO_2$ bond was incrementally stretched using geometry scanning, to obtain an energy profile of the reaction. For the rigid scan (figure 1.3), only the internal angle of the departing NO_2 and coordinates referencing its orientation relative to the rest of the molecule were allowed to relax. As the scan progressed, the NO_2 internal angle increased from 129.2° to 134.6°, at maximum separation of 5 Å from the bridging oxygen (Ox). This corresponds to the literature value for the $O-N-O$ internal angle (134.3°) confirming the formation of a $^{\cdot}NO_2$ radical.

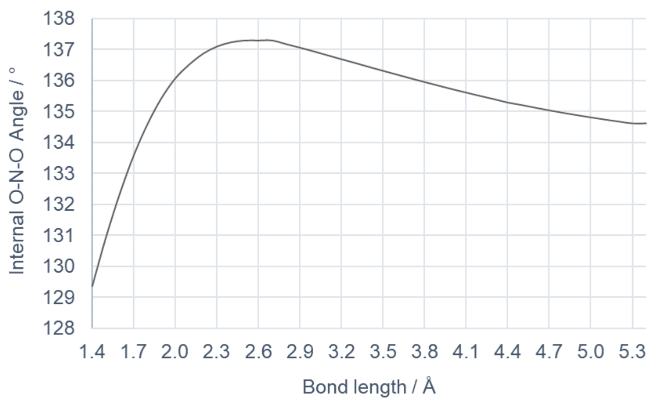

Figure 1.3: The relaxation of the $O-N-O$ internal angle as the NO_2 group is pulled away from the NC monomer during a rigid geometry scan of homolytic fission.

The values obtained for HNO_2 elimination of PETN follow the results given by Tsyshevsky much more closely. The energies fall within 5 kCal mol^{-1} and 6 kCal mol^{-1} for the

Gibbs free energy of reaction and activation barrier, respectively. This is within a reasonable margin of error for comparing with experimentally obtained values, though still larger than expected for those derived using the same method, basis and structure.

In the case of the NC monomer, both rigid and relaxed scans failed to capture the transition state (TS) for cleavage of the nitrate group via interaction with the α-hydrogen. A guess transition state was constructed based on the TS of the analogous reaction for PETN (figure 1.4b), and optimised to produce the structure of the correct imaginary vibration.

The pattern for the NC monomer resembles that found for PETN; homolysis is endothermic but with lower activation barrier, whilst HNO_2 elimination is exothermic, but with a much higher barrier. It is anticipated therefore, that the rate of homolytic fission will be faster, whilst HNO_2 loss will happen more slowly, whilst contributing to system heating and increasing acid concentration.

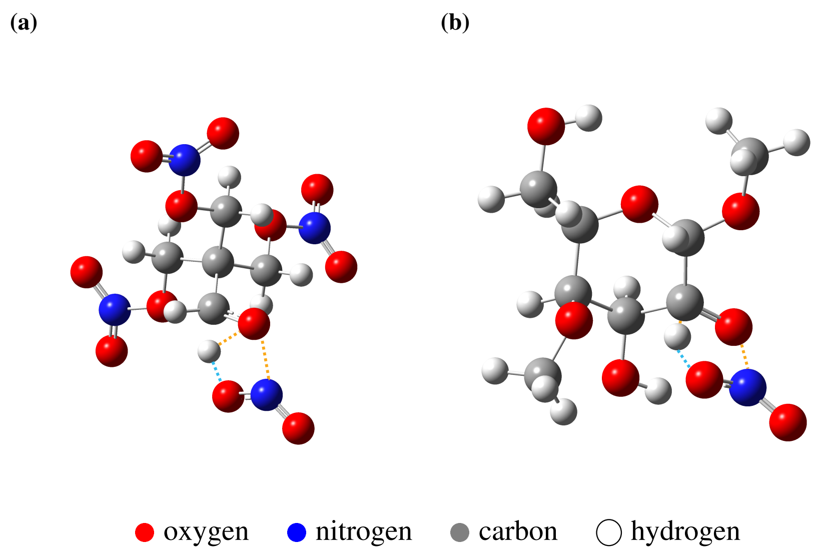

Figure 1.4: TS for the elimination of HNO_2 by removal of the α-hydrogen by the NO_2 leaving group in 1.4a PETN and 1.4b NC. Orange dashed lines indicate bonds breaking and blue dashed lines indicate bonds forming.

1.3.2 Acid hydrolysis mechanism

1.3.2.1 Protonation site

When in the presence of protic solvents, fast-exchange of protons is expected between the monomer and solvent. This process in glucose was studied computationally by Jebber and Liu *et al.* [19, 20]. The studies demonstrated that the most favourable protonation site in glucose was influenced by the orientation of the C6 side branch, whilst the lowest energy site for protonation is the oxygen of the C1 hydroxy group. The analogous group in the

NC monomer is the C1 capping group oxygen. The protonated NC monomer species are shown in figure 1.5. The bridging oxygen (Ox), the C1 capping group oxygen, and the interchangeable terminal nitrate oxygen sites (Ot) were protonated and their relative energies compared, to determine the site most likely to stabilise the proton at thermal equilibrium. Protonation also occurs on other sites in the molecule, such as at unsubstituted hydroxyl oxygen sites, the capping group oxygen on C4 and O1 in the glucose ring. Though it is a possibility that protonation at further sites in the monomer would contribute to degradation, these processes would occur *via* alternative mechanisms without the involvement of denitration. For the purposes of studying acid hydrolysis, only the sites peripheral to the nitrate leaving group were explored.

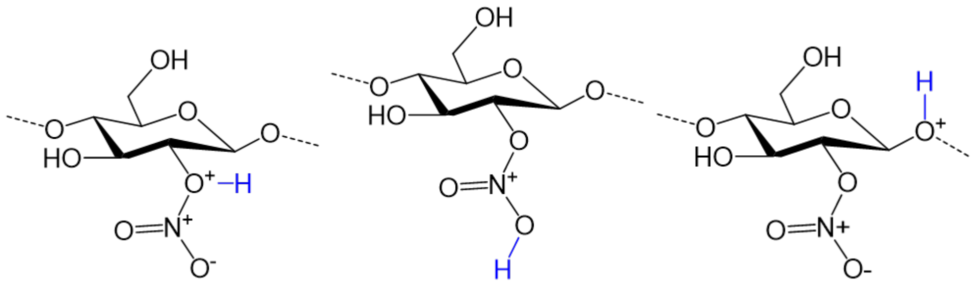

(a) Bridging **(b)** Terminal **(c)** Capping

Figure 1.5: Protonation sites on the NC monomer for hydrolysis of the nitrate at the C2 position.

Table 1.3: Free energies of protonation, for each of the oxygen sites of interest on CH_3CH_3 monomer of NC, nitrated at the C2 site.

Protonation site	ΔG_r /kcal mol^{-1}			
	ωB97X-D	PCM	B3LYP	PCM
Bridging	−26.04	4.03	−28.67	11.29
Terminal (Upper)	−29.85	24.29	−31.19	15.33
Terminal (Lower)	−20.54	10.44	−22.41	11.67
Capping	−29.85	3.62	−31.19	−1.16

It can be seen that the bridging and capping values are very similar using both ωB97X-D and B3LYP. Inspection of the geometries revealed that the optimised bridging and capping structures were extremely similar (figures 1.5a and 1.5c). The difference in energies between the gaseous and implicit solvent values are explained by the instability of H_3O^+ in vacuum, where it prefers to lose the proton and exist as water, whereas when solvated, its positive charged is stabilised. Thus, the energy gained from losing the proton is negative, when in solution. Water as the protonating species was attempted, by optimi-

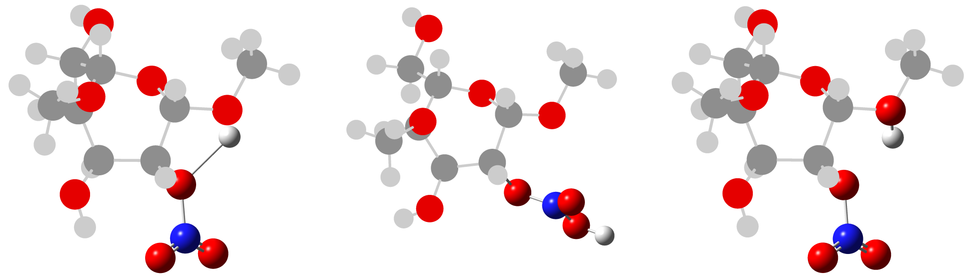

(a) Bridging **(b)** Terminal **(c)** Capping

Figure 1.6: Optimised protonated NC monomer structures, showing interaction between the proton on the bridging site with the capping group oxygen.

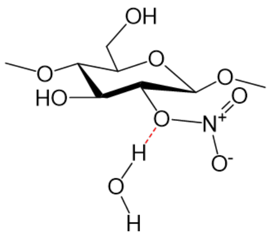

Figure 1.7: The attempted geometry of a single water molecule in coordination with the NC monomer.

sation of one, two and three water molecules in coordination with the nitrate site in the NC monomer, however no stable complex could be isolated. It is anticipated that a much larger network of waters around both the regions surrounding the nitrate moiety, and the wider molecule, are be required to achieve a stable water coordination structure. This would be of interest for further investigation into the mechanism of neutral hydrolysis (figure **??**). Evaluation of the energy of protonation at each site found that the bridging and capping sites most likely. However, all possible structures will be explored for the subsequent denitration stage.

1.3.2.2 Denitration by hydrolysis

Following the protonation step, possible transition states for the removal of the nitrate were investigated. Direct dissociation of NO_2 from the protonated species was explored, along with the simultaneous approach of a proton and cleavage of the NO_2 (figure 1.8). The scan of the proton moving towards the bridging site was also completed to gain insight to the energy profile of the process. The relaxed PES scan of NO_2 removal from ethyl nitrate protonated at the bridging site was used as a preliminary test for the mechanism of

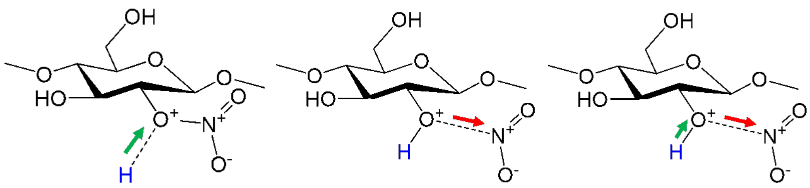

Figure 1.8: The scanned coordinates of a) proton approach, b) dissociation of NO_2 and c) concerted protonation and NO_2 dissociation.

denitration following protonation (figure 1.9). Unrestricted ωB97X-D was used, with 20 steps of 0.1 Å, however bond dissociation was not illustrated in the energy profile even when extending the scan distance to a maximum of 6.4 Å. Instead, a steady increase in the energy was observed. It can be seen that as the nitrate departs, the whole molecule rotates and the NO_2 leaving group aligns with the hydroxyl in an orientation suitable for formation of a peroxy group. The internal angle of the leaving group increases to 180°, confirming that NO_2 leaves as NO_2^+. This was the expected outcome for hydrolysis, as it is anticipated that the NO_2^+ will further react to produce acids conducive to further hydrolysis. Proposed

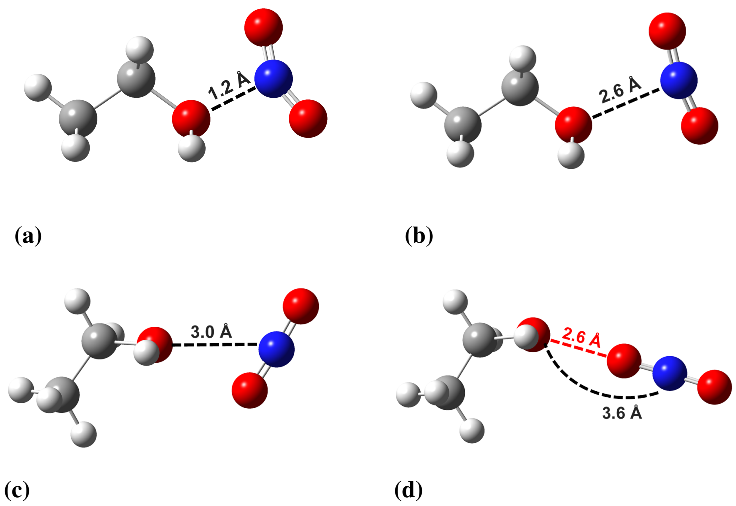

Figure 1.9: Geometries from steps 1, 7, 11 and 26 of the PES scan of ethyl nitrate (EN)

4-membered ring and 6-membered ring TS were investigated in order to determine whether they energetically and geometrically reasonable structures. Optimisations were attempted with both full geometry relaxation, and various frozen coordiate schemes for each proposed TS. The R groups were simplified to methyl nitrate (R = CH_3) in effort to limit degrees of freedom during optimisation of the TS structures, however no fully relaxed structures were able to achiever convergence. Fixing of the bulk molecule with relaxation only around the

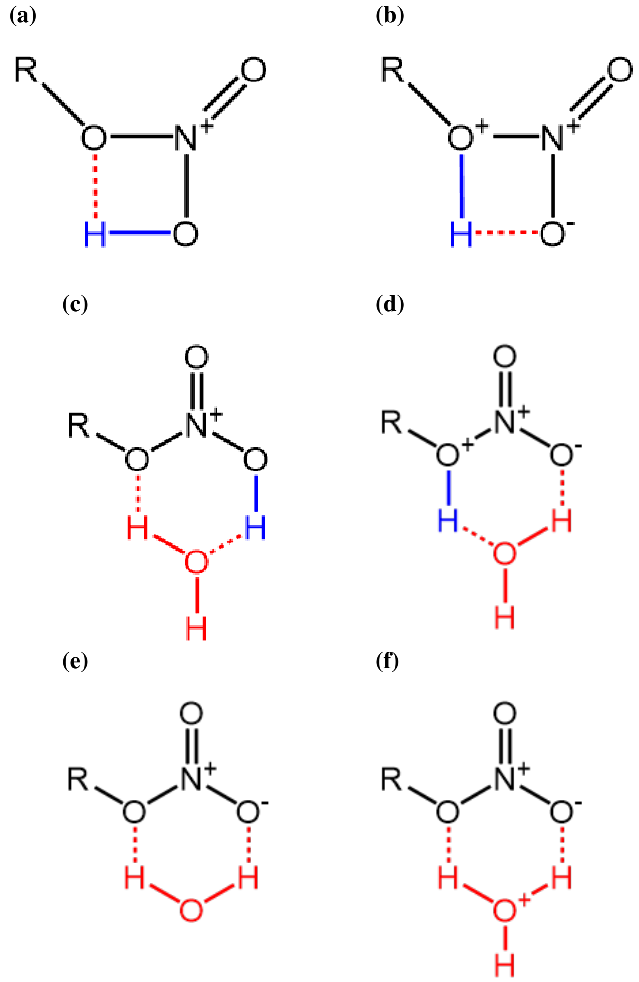

Figure 1.10: Proposed 4-member and 6-member ring transition states for the denitration of a nitrate ester, under various hydrolytic conditions. R = CH_3 in the case of methyl nitrate, R = CH_2CH_3 in the case of ethyl nitrate and R = $(H_3CO)_2C_6H_9O_3$ for the monomer.

nitrate and coordinating species, or relaxation of the wider molecule with fixed coordinates around the nitrate, allowed sequential optimisation of different moieties, increasing chances of global energy minimisation. It was possible to optimise the 4-membered ring bridging TS on the NC monomer with frozen TS ring geometry *via* preliminary optimisation of the ring structure with methyl nitrate. The optimised ring geometry was then placed on the monomer, with fixing of thee coordinates, allowing the remainder of the molecule to relax. A rigid scan was then performed of the 4-membered ring transition starting from the bridging site protonated monomer. It was revealed that as the nitrate moved away from the system, the proton moved to the capping group site rather than remain on the bridging oxygen as a hydroxyl, as was expected. Instead, a ketone group was formed between the bridging oxygen and the ring. At subsequent steps, the ketone group causes the C2 - C3 bond to elongate and break. The scan eventually revealed the NO_2 leaving group reclaiming the proton from the capping group oxygen, leading to ring fission. The activation and kinetic barrier involved in ring fission is much higher than that of denitration; a study on the acid hydrolysis of glucose and xylose demonstrated that ring-opening intermediates were either extremely short lived, or not observed at all [**?**]. The open-chain product of the scan is likely due to the geometric constraints placed on the geometry of the departing NO_2 group, rather than a physically energetic process. However, it sheds light on the scheme by which ring fission occurs, with has been implied in previous work involving the formation of a ketone at earlier stages of the reaction. Attempts to isolate the other TS structures were

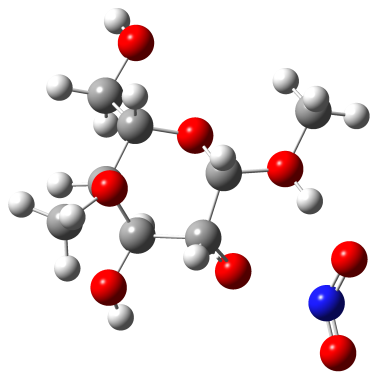

(a) In the initial stages of increasing O$-$$NO_2$ distace, the proton moves to the capping group.

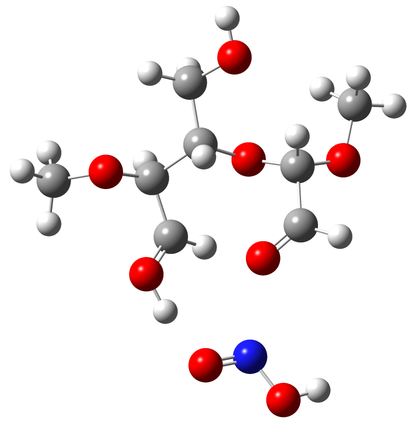

(b) At separation of over 3.3 Å, the C2 –C3 bond breaks leading to ring fission. The proton then moves back onto NO_2 .

Figure 1.11: Relaxed scan of NO_2 departure, starting with the 4-membered ring structure.

unsuccessful, even when simplifying the side chain to methyl nitrate and applying implicit solvent in the case it stabilised the charges on the strained structures.

1.4 Summary

Thermolytic cleavage of the nitrate was modelled *via* homolysis and elimination of HNO_2. In the case of PETN it was found that the reaction energies were lower than expected when comparing with literature values. This may be due to differing geometries of the modelled reaction products, or due to the separate evaluation of the pentaerythritol trinitrate (PETRIN) radical and $^{\cdot}NO_2$ engergies, where they should have remained in complex following the reaction. The same process was repeated for the NC monomer, singly nitrated at the C2 site. The energy of homolytic fission was in good agreement with the expected value based on the outcome of the PETN product. PES scans of homolysis confirmed the loss of $^{\bullet}NO_2$ for both the case of PETN and the NC monomer.

The elimination of HNO_2 *via* intramolecular α-H attack was also explored. Compared to the homolysis reaction, the energy of reaction and activation energy values gave better agreement to literature in the case of PETN. Calculated NC values were also within anticipated values, based on the reaction for PETN. PES scans were unable to location a TS for the NC monomer, however, a successful guess geometry was generated based on the analogous structure in the reaction for the PETN. Enthalpies of reaction energies show that this processes was more exothermic in the case of NC, then for PETN.

The protonation sites on the NC monomer were probed for the most favourable position. It was found that the bridging site was energetically preferred, though inspection of the optimised geometry showed that it was very close to that of protonation at the capping site. As protonation and subsequent reaction would more likely lead to chain scission in the case of capping protonation, this avenue was disregarded in further studies focussing on the acid hydrolysis pathway. Optimisation of [water - monomer] and [hydronium - monomer] complexes were attempted, in order to obtain information on the nature and orientation of the protonation complex. However, it was not possible to isolate any stable structures, implying that a larger stabilising network of waters is likely required.

Removal of NO_2 from the protonated analogues of ethyl nitrate and the NC monomer was scanned using a variety of rigid and relaxed PES schemes. In the removal of NO_2 from ethyl nitrate the released of NO_2^+ was indicated by the change of geometry around the nitrate from bent to linear, as the $O-NO_2$ bond elongated. Rotation of the remaining ethanol and complexed NO_2^+ showed orientation suitable for formation of a peroxide. This rotation was not observed in the case of the monomer, however the leaving group still presented as NO_2^+. 4 and 6 membered TS were also tested for the denitration reaction. Unexpectedly, it was found that none of the 6-membered ring structures could be isolated, regardless of prior protonation of concerted protonation-denitration. In the case of the bridging-protonated NC with formation of the 4-membered ring TS at the C2 nitrate, it was possible to relax the NC monomer structure around the ring so long as the ring geometry itself was frozen. As the leaving group moved further from the remainder of the molecule, the hydroxyl group located at C2 formed a ketone, losing the proton to the departing NO_2^+, to form HNO_2 in later stages of the scan. Eventually ring fission occurred, as the HNO_2 move sufficient distance away, and the formation of the ketone forced the adjacent $C-C$ bond in the ring to stretch, and then break.

Bibliography

[1] Jimmie C. Oxley. A survey of the thermal stability of energetic materials, jan 2003.

[2] M F Foltz. Aging of pentaerythritol tetranitrate (PETN). *LLNL-TR-415057, Lawrence Livermore National Laboratory, Livermore, CA, USA*, apr 2009.

[3] T. Shepodd, R. Behrens, D. Anex, D. Miller, and K. Anderson. Degradation chemistry of PETN and its homologues. Technical report, Sandia National Laboratories (SNL), Albuquerque, NM, and Livermore, CA (United States), nov 1997.

[4] Roman V. Tsyshevsky, Onise Sharia, and Maija M. Kuklja. Thermal Decomposition Mechanisms of Nitroesters: Ab Initio Modeling of Pentaerythritol Tetranitrate. *The Journal of Physical Chemistry C*, 117(35):18144–18153, sep 2013.

[5] Mohammed Moniruzzaman, John M. Bellerby, and Manfred A. Bohn. Activation energies for the decomposition of nitrate ester groups at the anhydroglucopyranose ring positions C2, C3 and C6 of nitrocellulose using the nitration of a dye as probe. *Polymer Degradation and Stability*, 102:49–58, apr 2014.

[6] I. Rodger and J. D. Mcirvine. The decomposition of spent PETN nitration acids. *The Canadian Journal of Chemical Engineering*, 41(2):87–90, apr 1963.

[7] Torbjórn Lindblom. Reactions in stabilizer and between stabilizer and nitrocellulose in propellants. *Propellants, Explosives, Pyrotechnics*, 27(4):197–208, sep 2002.

[8] Hermann N. Volltrauer and Arthur Fontijn. Low-temperature pyrolysis studies by chemiluminescence techniques real-time nitrocellulose and PBX 9404 decomposition. *Combustion and Flame*, 41(C):313–324, jan 1981.

[9] M. Edge, N.S. Allen, M. Hayes, P.N.K. Riley, C.V. Horie, and J. Luc-Gardette. Mechanisms of deterioration in cellulose nitrate base archival cinematograph film. *European Polymer Journal*, 26(6):623–630, jan 1990.

[10] Maria Ángeles Fernández de la Ossa, María López-López, Mercedes Torre, and Carmen García-Ruiz. Analytical techniques in the study of highly-nitrated nitrocellulose. *TrAC Trends in Analytical Chemistry*, 30(11):1740–1755, dec 2011.

[11] John W. Baker and D. M. Easty. Hydrolytic decomposition of esters of nitric acid. Part I. General experimental techniques. Alkaline hydrolysis and neutral solvolysis of methyl, ethyl, isopropyl, and tert.-butyl nitrates in aqueous alcohol. *Journal of the Chemical Society (Resumed)*, 1952(0):1193–1207, 1952.

[12] N. Binke, L. Rong, Y. Zhengquan, W. Yuan, Y. Pu, Hu Rongzu, and Y. Qingsen. Studies on the Kinetics of the First Order Autocatalytic Decomposition Reaction of Highly Nitrated Nitrocellulose. *Journal of Thermal Analysis and Calorimetry*, 58(2):403–411, 1999.

[13] M. A. Zayed, Salah E M El-Begawy, and Hossam E S Hassan. Enhancement of stabilizing properties of double-base propellants using nano-scale inorganic compounds. *Journal of Hazardous Materials*, 227-228:274–279, aug 2012.

[14] Djalal Trache and Ahmed Fouzi Tarchoun. Stabilizers for nitrate ester-based energetic materials and their mechanism of action: a state-of-the-art review. *Journal of Materials Science*, 53(1):100–123, jan 2018.

[15] E. Camera, G. Modena, and B. Zotti. On the Behaviour of Nitrate Esters in Acid Solution. II. Hydrolysis and oxidation of nitroglycol and nitroglycerin. *Propellants, Explosives, Pyrotechnics*, 7(3):66–69, jun 1982.

[16] K. S. Hu, A. I. Darer, and M. J. Elrod. Thermodynamics and kinetics of the hydrolysis of atmospherically relevant organonitrates and organosulfates. *Atmospheric Chemistry and Physics*, 11(16):8307–8320, aug 2011.

[17] V. G. Matveev and G. M. Nazin. Stepwise Degradation of Polyfunctional Compounds. *Kinetics and Catalysis*, 44(6):735–739, nov 2003.

[18] S. Miertuš, E. Scrocco, and J. Tomasi. Electrostatic interaction of a solute with a continuum. A direct utilizaion of AB initio molecular potentials for the prevision of solvent effects. *Chemical Physics*, 55(1):117–129, feb 1981.

[19] Kimberly A. Jebber, Kui Zhang, Carolyn J. Cassady, and Alice Chung-Phillips. Ab initio and experimental studies on the protonation of glucose in the gas phase. *Journal of the American Chemical Society*, 118(43):10515–10524, 1996.

[20] Dajiang Liu, Mark R. Nimlos, David K. Johnson, Michael E. Himmel, and Xianghong Qian. Free energy landscape for glucose condensation reactions. *Journal of Physical Chemistry A*, 114(49):12936–12944, dec 2010.